scientific reports

Check for updates

OPEN

Synthesis, characterization, Hirshfeld surface analysis, antioxidant and selective β-glucuronidase inhibitory studies of transition metal complexes of hydrazide based Schiff base ligand

Farzia[1], Sadia Rehman[1]✉, Muhammad Ikram[1]✉, Adnan Khan[2]✉, Rizwan Khan[3], Mutasem Omar Sinnokrot[4], Momin Khan[1], Abdullah F. AlAsmari[5], Fawaz Alasmari[5] & Metab Alharbi[5]

The synthesis of N′-[(4-hydroxy-3-methoxyphenyl)methylidene] 2-aminobenzohydrazide (H-AHMB) was performed by condensing O-vanillin with 2-aminobenzohydrazide and was characterized by FTIR, high resolution ESI(+) mass spectral analysis, ^{1}H and ^{13}C-NMR. The compound H-AHMB was crystallized in orthorhombic *Pbca* space group and studied for single crystal diffraction analysis. Hirshfeld surface analysis was also carried out for identifying short interatomic interactions. The major interactions H…H, O…H and C…H cover the Hirshfeld surface of H-AHMB. The metal complexes [M(AHMB)n] where M = Co(II), Ni(II), Cu(II) and Zn(II) were prepared from metal chlorides and H-AHMB ligand. The bonding was unambigously assigned using FTIR and UV/vis analysis. The synthesized ligand H-AHMB and its metal complexes were studied for *β*-glucuronidase enzyme inhibition. Surprisingly the metal complexes were found more active than the parent ligand and even the standard drug. Zn-AHMB shown IC_{50} = 17.3 ± 0.68 µM compared to IC_{50} = 45.75 ± 2.16 µM shown by D-saccharic acid-1,4-lactone used as standard. The better activity by Zn-AHMB implying zinc based metallodrug for the treatment of diseases associated with *β*-glucuronidase enzyme. The DPPH radical scavenging activities were also studied for all the synthesized compounds. The Co-AHMB complex with IC_{50} = 98.2 ± 1.78 µM was the only candidate to scavenge the DPPH free radicals.

Molecular target therapy is the most popular approach in the field of medicinal chemistry to design drugs with improved therapeutic effects. Due to their importance in numerous biological processes, glycosyl hydrolases (GHs) are one of these targets. GHs inhibitors are involved in antiviral, anticancer and antidiabetic drug development[1–3]. A member of the group of GHs, *β*-glucuronidase (GLU) is an enzyme that is present in the endoplasmic reticulum, bodily fluids, and mammalian lysosomes[4]. It has also been observed in plants, fishes, insects and mollusks and catalyzes the conversion of *β*-D-glucuronides to their corresponding aglycone and *β*-D-glucuronic acid through hydrolysis as shown in Scheme 1.

[1]Department of Chemistry, Abdul Wali Khan University, Mardan, Pakistan. [2]School of Physics & the Key Laboratory of Weak Light Nonlinear Photonics, Ministry of Education, Nankai University, Tianjin 300071, People's Republic of China. [3]Department of Zoology, Abdul Wali Khan University, Mardan, Pakistan. [4]College of Arts and Sciences, American University of Iraq-Baghdad, Airport Road Baghdad, Baghdad, Iraq. [5]Department of Pharmacology and Toxicology, College of Pharmacy, King Saud University, 11451 Riyadh, Saudi Arabia. ✉email: sadia@awkum.edu.pk; ikram@awkum.edu.pk; adnanphyzx@nankai.edu.cn

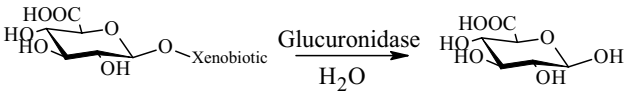

Scheme 1. Conversion of *β*-D-glucuronides to *β*-D-glucuronic acid.

β-Glucuronides enzyme is overly expressed in various types of cancers like breast[5], cervical[6], colon[7], lung[8], renal carcinoma and leukemia[9]. It has been found that *β*-GLU also effect other organs when overly expressed causing certain infections like urinary tract infection[10], diabetes[11], neuropathy[12], HIV[12] and rheumatoid arthritis[13]. *β*-glucuronidase enzyme has been shown to be released abnormally in chronic rheumatoid arthritis (RA). As a result of the RA's impact on the blood vessels, heart, lungs, muscles, and joints, bone deformities and osteoporosis develops[14].

Therefore, inhibition of *β*-glucuronidase enzyme is deemed as potential molecular target for designing anticancer, anti-inflammatory, antidiabetic and antineuropathic drug[15–20]. Plethora of potential inhibitors of *β*-Glucuronides exists comprising of both organic and coordination derivatives. D-saccharic acid-1,4-lactone is one of the successful inhibitor[21] of *β*-glucuronidase with $IC_{50} = 3.6$ μM[22]. Similarly, 2,5-di-*O*-acetyl-D-glucaro-1,4:6,3-Dilactone and D-glucurono-*γ*-lactone have also been studied with marked inhibition of the *β*-glucuronidase enzyme[23]. A piperazine diamine derivative has been found with $IC_{50} = 0.08$ μM[24,25]. It was suggested after SAR studies that the nucleophilic NH moiety impart greater efficacy to the molecule. Therefore, in recent study we are reporting the hydrazide derivative 2-amino-*N*′-[(*E*)-(4-hydroxy-3-methoxyphenyl) methylidene]benzohydrazide synthesized by reacting p-vanilline and 2-aminobenzohydrazide. Furthermore, substantial effects were observed by combining the active compounds with metal centers to produce metal complexes[26–34]. Metal complexes offer better activities over the conventional drugs[21,35–57] as illustrated by copper (II) derivative of H–NMDP which revealed antiproliferation effect against A172 and LN229[58]. Similarly, aminoacid derived ligand H-HMAC and its Co(II), Ni(II), Cu(II) and Zn(II) metal complexes were studied for different enzyme inhibitory activities viz; urease, *α-Chymotrypsin,* Acetylcholinesterase (AChE) and butyrylcholinesterase[59], and xanthine oxidase along with antioxidant potentials[60]. It was found that the ligand combined with zinc was found selectively inhibiting the urease enzyme with $IC_{50} = 0.049 \pm 0.01$ μM. The same complex was also involved in inhibiting the xanthine oxidase with $IC_{50} = 0.7 \pm 0.01$ μM. Therefore, it can be concluded that Schiff base metal complexes play a very important role in inhibiting enzymatic activities and biological activities. As a result, the current study is primarily concerned with synthesizing the metal complexes of the Schiff base ligand that is produced from hydrazides. The *β*-glucuronidase inhibition of the products was evaluated.

Experimental

Chemicals and reagents

Chemicals and solvents used in the current work were obtained in their purest forms from different local suppliers like Metal(II) acetates (where metal(II) = Co, Ni, Cu and Zn) from Riedel-de-Haen, Salicylaldehyde from Acros Organics, solvents from Merck and Sigma Aldrich. Metal salts were dried in a vacuum oven for 3–4 h at 80–100 °C before reaction. 2-aminobenzohydrazine was prepared using the previously reported procedure. The reaction environment was kept inert, and the manipulations were carried out in Schlenk line.

Synthesis of N′-[(4-hydroxy-3-methoxyphenyl)methylidene] 2-aminobenzohydrazide (H-AHMB)

Benzohydrazide ligand was synthesized as described in the previously reported work[61]. 10 mmol of benzohydrazide was reacted 10 mmol of 4-hydroxy-3-methoxybenzaldehyde in 10 cm^3 of distilled methanol and the mixture was stirred for about an hour. Yellow color solution was obtained which was concentrated using rotary evaporator. The single crystals were obtained from the concentrated solution in THF.

Yoeld: 84%, Color: Yellow, IR: cm^{-1} 3369 (s), 3215.34(b), 1641.42(s), 1616.35(m), 1604.77(s), 1489.05(m), 1456.26(s), 1408.04(s), 1361.74(s), 1300.02(s), 1234(s), 1203.58(w), 1170(s), 1153.43(s), 1097.50(s), 948.98(s), 925.83(m), 862.18(s), 855(s), 820(s), 770(s), 760(s), 748.38(s), 701(s), 696.30(s), 650.01(s), 590.22(s), 553.57(m). Elemental analysis: ($C_{22}H_{19}N_3O_2$) Calcd. C(63.15%), H(5.30%), N(14.73%), Found. C(63.69%), H(5.56%), N(14.46%), EI-MS: m/z (%) 286.1192 $[C_{15}H_{16}N_3O_3]^+$, ^{1}H-NMR 2.1(s, CH=N), 2.5(s,$CDCl_3$), 3.4(s, NH_2), 3.8(s, OCH_3), 6.4(s, RCONH), 6.6(t, H17), 6.7(d, H4), 6.8(d, H16), 7.1(d, H19), 7.2(t, H18), 7.3(s, H2), 7.6(d, H5), 8.3 (s, OH), ppm. $^{13}C\{^1H\}$-NMR 56.34 (OCH_3),109.75 (CH, C17), 111.83 (C, C3), 115.44(CH, C18), 117.11(CH, C4), 122.81(CH, C2), 126.75(CH, C16), 132.90(CH, C19), 134.53 (C, C15), 148.23(C, C20), 148. 85(CH, C5), 149.62(CH, CH=N), 150.70(C, C–OH),165.93 (C, C=O)ppm.

Synthesis of transition metal complexes {M-AHMB where M = Co^{2+}, Ni^{2+}, Cu^{2+}, and Zn^{2+} as chlorides}

In a minimal volume of dry methanol, 30 mmol of the ligand (H-AHMB) was combined with 15 mmol of the salts of the divalent metals {Co(II), Ni(II), Cu(II), and Zn(II)}, and the combination was agitated for 6 to 8 h at room temperature. Following the development of metal complexes or adducts, they were filtered out and washed with dry n-hexane.

Cobalt adduct with N′-[(4-hydroxy-3-methoxyphenyl)methylidene] 2-aminobenzohydrazide [Co-AHMB]
Greyish green, Yield: 66%, IR: cm^{-1} 3369.64(s), 3180.62(b), 1641.42(s), 1616.35(m), 1604.77(s), 1489.05(m), 1456.26(s), 1408.04(s), 1361.74(s), 1300.02(s), 1240,23(s), 1200(w), 1161.15(w), 1153.43(s), 1097.50(s), 980(s), 950.91(s), 910(m), 867.97(s), 855(s), 820(s), 770(s), 760(s), 748.38(s), 701(s), 696.30(s), 650.01(s), 630.72(w), 590.22(s), 553.57(m), 499.56(s), 491.85(s), 459.06(s), 449.41(s), $\lambda_{max} = 620$ nm ($\varepsilon = 16.0$ M^{-1} cm^{-1}, $^2A_2 \rightarrow {}^2B_1$), $\mu_{eff} = 3.9$ B.M.

Nickel adduct with N′-[(4-hydroxy-3-methoxyphenyl)methylidene] 2-aminobenzohydrazide [Ni-AHMB]
Emerald green, Yield: 74%, IR: cm^{-1} 3292.49(b), 1635(s), 1614.425(m), 1598.99(m), 1573.91(w), 1489.05(m), 1456.26(s), 1390.68(w), 1360(w), 1300(w), 1271.09(m), 1234.44(m), 1203.58(w), 1153.43(s), 1097.50(s), 980(s), 950.91(s), 910(m), 860.25(s), 855(m), 820(w), 760(w), 746.45(s), 721.38(w), 690.52(s), 646.15(w), 613.36(s), 576.72(s), 549.71(s), 499.56(s), 491(s), 462.92(s), $\lambda_{max} = 710$ nm ($\varepsilon = 26.9$ M^{-1} cm^{-1}, $^1A_1 \rightarrow {}^1A_2$), $\mu_{eff} = 2.9$ B.M.

Copper adduct with N′-[(4-hydroxy-3-methoxyphenyl)methylidene] 2-aminobenzohydrazide [Cu-AHMB]
Dark green, Yield: 76%, IR: cm^{-1} 3600(b), 3290(m), 3000(m), 1610.56(s), 1600.92(s), 1571.99(w), 1537.27(s), 1489.05(m), 1463.97(s), 1442.75(s), 1430(s), 1379.10(s), 1360(w), 1300(w), 1290.38(s), 1246.02(s), 1193.94(s), 1151.50(s), 1097(s), 1053.13(s), 980(s), 950.91(s), 918(s), 873.75(s), 854.47(s), 817.82(s), 760(s), 746.45(s), 690.52(s), 646(s), 610(s), 596(s), 550(s), 490(s), $\lambda_{max} = 820$ nm ($\varepsilon = 18.9$ M^{-1} cm^{-1}, $^2E \rightarrow {}^2T_2$), $\mu_{eff} = 1.9$ B.M.

Zinc adduct with N′-[(4-hydroxy-3-methoxyphenyl)methylidene] 2-aminobenzohydrazide [Zn-AHMB]
Yellowish orange, Yield: 73%, IR: cm^{-1} 3369.64(s), 3219.19(b), 1639.49(s), 1616.35(s), 1604.77(s), 1489.05(s), 1456.26(s), 1435.04(s), 1408.04(s), 1359.82(s), 1300(w), 1271.09(m), 1238(s), 1230.58(w), 1203.58(s), 1170(s), 1153.43(s), 1097.50(s), 1037.70(s), 970(s), 948.98(s), 925.83(s), 867.97(s), 855(s), 820(s), 800(s), 750(s), 721.38(s), 694.37(s), 646.15(s), 630.72(m), 586.36(s), 553.57(s), 437.84(s).

Instrumentation

Varian Elementar II instrument was used for finding the elemental composition (experimental). Vario 6, Analytic Jena atomic absorption spectrophotometer was used for the metal ion content. PerkinElmer spectrophotometer version 10.4.00 with serial number 95120 made in Lliantrisant, UK was used for recording the ATR spectra of all the samples. ^{1}H-NMR and ^{13}C-NMR spectra of the Hydrazide Schiff base ligand was found by BRUKER advance III 400 spectrometer.

Crystal structure determination

A glass fiber was mounted with crystals of the ligand in innocuous paraffin oil. On oxford diffractometer using graphite-monochromated Mo-K radiation ($\lambda = 0.71073$), data were collected at 170 K. The structures were solved using Charge Flipping with the olex2.solve[62,63] and refined with the olex2.refine[62]. The additional information file contains crystallographic information, and the structure was sent to the CCDC. via quoting the CCDC-number 2281686 for H-AHMB, data may be requested from the Cambridge Crystallographic Data Centre via FAX (+44-1223-336-033), email (deposit@ccdc.cam.ac.uk), or their online interface (at http://www.ccdc.cam.ac.uk).

Hirshfeld surface analysis and 2D fingerprint plot

Crystal Explorer 21.5 was used for computing short contacts between neighbouring molecules using the refined cif of H-AHMB. Hirshfeld surfaces in the crystal lattice were investigated. The two-dimensional (2D) fingerprint plot of short interatomic contacts and the interaction energies were envisaged. The colour gradient (red to blue) were used to represent the parameters derived from the normalized contact distance d_{norm} described in terms of the van der Waals radii (vdW) of atoms, d_i and d_e parameters. The 2D finger plots derived between d_i and d_e within the range 0.6–2.8 Å were used to derive the set of interactions. Deep red colour on the represent the short interatomic interactions while the light red spots represent the poor interactions and the blue colour spots represent non-interacting regions. The Hirshfeld surface's distances from the neighboring atomic centers are displayed by the parameters used on 2D fingerprint plots between *di* and *de*.

Biological studies

β-Glucuronidase inhibitory activity
β-Glucuronidase inhibitory activity by hydrazide Schiff base ligand (H-AHMB) and its metal (II) complexes was investigated using standard procedure. P-Nitrophenol produced as a result of reaction from the substrate during the procedure was measured spectrophotometrically at 405 nm to evaluate the *β*-glucuronidase activity. According to the procedure 185 µL of 0.1 M acetate buffer, 5 µL compound to be tested and 10 µL of enzyme solution were mixed and incubated at 37 °C for 30 min. SpectraMax plus 384, Molecular Devices, USA was used to read on a multiplate reader at 405 nm after the addition of 0.4 mM p-nitrophenyl-*β*-D-glucuronide (50 µL). All experiments were performed in triplicate.

2,2-diphenyl-1-picrylhydrazyl) (DPPH) radical scavenging studies
The synthetic Schiff base ligand and its metal complexes were tested for their ability to scavenge DPPH radicals using the methodology described by Soare, Dinis, Cunha, and Almeida in 1997[64]. Initially, 1 mL of 0.2 mM DPPH dissolved in methanol was combined with 0.1 mL of each sample at 250, 500, 750, and 1000 g/mL concentrations. For 20 min, the reaction mixture was kept at 28 °C and kept in the dark. Methanol served as the control, which had all the components but no sample. A UV/Vis spectrophotometer was used to detect the absorbance at 517 nm

in order to assess the DPPH radical scavenging activity. For comparison, the DPPH radical scavenging capacity of ascorbic acid was also determined.

$$\%\ Inhibition\ effect = \frac{A_c - A_s}{A_c} \times 100$$

A_c = Absorbance by the control, A_s = Absorbance by the sample[37].

Results and discussion

The ligand H-AHMB and its metal derivatives were synthesized and characterized using different analytical and spectroscopic techniques. The elemental composition is in agreement with the formation of the ligand H-AHMB after the reaction of vanillin with benzohydrazide. The percent composition of the complexes revealed the formation of the metal derivatives of the H-AHMB ligand. Mass spectrum of the H-AHMB (as shown in supplementary file) also revealed the molecular ion peak at the m/z = 286.1201 for $[C_{15}H_{16}N_3O_3]^+$.

Structural studies of H-AHMB ligand

The single crystals of the synthesized hydrazide derived Schiff base ligand H-AHMB was structurally characterized using single crystal diffraction analysis (Fig. 1). The crystal data as given in Table 1 revealed orthorhombic, *Pbca* space group. The Schiff base linkage in H-AHMB {C4-N10 = 1.2946(6) Å (Table 2)} is comparatively longer than similar bond lengths in amino acid derivative (H-HMAC) with C9-N8 = 1.2910 Å[60] and in cyclized hydrazide derivative (H-HHAQ) with C8-N9 = 1.275(9)Å[61].

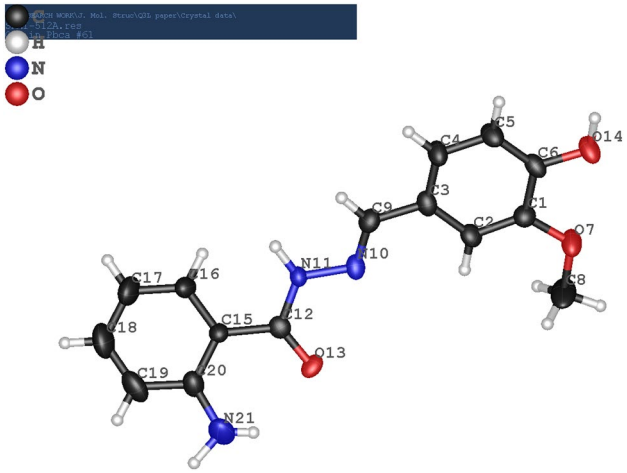

Figure 1. Molecular structure of H-AHMB.

Compound	H-AHMB
Molecular formula	$C_{15}H_{15}N_3O_3$
Formula mass	898.91
Temp.	170(2) K
λ	0.7107 Å
Crystal system, space group	Orthorhombic, *Pbca*
Unit cell dimensions	a = 16.092 (2) Å, α = 90° b = 7.9264 (8) Å, β = 90° c = 22.901 (3) Å, γ = 90°
V	2921.0 (6) Å^3
Θ range for data collection	3.1–27.0°
Limiting indices	0 < = h < = 19, 0 < = k < = 10, 0 < = l < = 20
Measured reflections	5182
Independent reflections	2750
R_{int}	0.076
Refinement method	Full-matrix least-squares on F^2
Data/restraints/parameters	2750/0/217
$R[F^2 > 2\sigma(F^2)]$	0.092, wR(F^2) = 0.177

Table 1. Crystal data and structure refinement parameters for H-AHMB.

Selected bond lengths of the H-AHMB Schiff base ligand			
Moiety	**Bond length, Å**	**Moiety**	**Bond length, Å**
O13—C12	1.248 (5)	O7—C1	1.375 (5)
O14—C6	1.360 (5)	O7—C8	1.425 (7)
N10—C9	1.294 (6)	C12—C15	1.474 (6)
C20—C19	1.410 (7)	C15—C16	1.397 (6)
C20—N21	1.362 (7)	C3—C2	1.400 (6)
N11—N10	1.389 (5)	C3—C9	1.450 (7)
N11—C12	1.341 (6)	C3—C4	1.388 (6)
Selected bond angles of the H-AHMB Schiff base ligand			
Moiety	**Bond angle, °**	**Moiety**	**Bond angle, °**
C12—N11—N10	119.1 (4)	N10—C9—C3	122.4 (4)
C4—C3—C2	119.3 (5)	C5—C6—O14	123.6 (5)
C4—C3—C9	118.4 (4)	C1—C6—O14	117.0 (4)
C9—N10—N11	114.2 (4)	C8—O7—C1	117.2 (4)
C19—C20—C15	118.1 (5)	O7—C1—C2	125.1 (4)
N21—C20—C15	123.8 (5)	O7—C1—C6	113.9 (4)
N21—C20—C19	118.0 (6)	C15—C12—N11	115.3 (4)
N11—C12—O13	122.0 (4)	C15—C12—O13	122.7 (4)

Table 2. Selected bond lengths and bond angles of the H-AHMB (Å, °).

The plane produced by C12-C15-C20-C19-C18-C17-C16 is twisted by 44.35° than the plane produced by C1-C2-C3-C4-C5-C6-C9-N10-N11 due to the formation of Schiff base linkage at C9-N10 moiety. This twist is also responsible for the comparative longer bond distance of the C=N moiety. The bond angle for C12—N11—N10 is 119.1 (4)° and for N10—C9—C3 is 122.4 (4)° is also supporting the aforementioned twist. Further support is also revealed from the bond angle of C4—C3—C9 which is 118.4 (4)° as may be seen in Table 2. The crystal lattice is produced by intermolecular hydrogen bonding of 1.745 Å between O14-H14…..O13 comparatively longer than similar bond distance as may be seen in amino acid derivative (H-HMAC) with a distance of 1.687 Å for O22-H23. The crystal packing diagram is shown in Fig. 2.

NMR study

The ligand H-AHMB was also characterized using ^{1}H-NMR and ^{13}C-NMR (figure 1S and 2S). ^{1}H-NMR of H-AHMB revealed representative peaks at their respective positions of the spectrum. A singlet at 2.1 ppm was assigned to the azomethine linkage. Another singlet at 3.4 ppm was assigned to the amine group. The amide

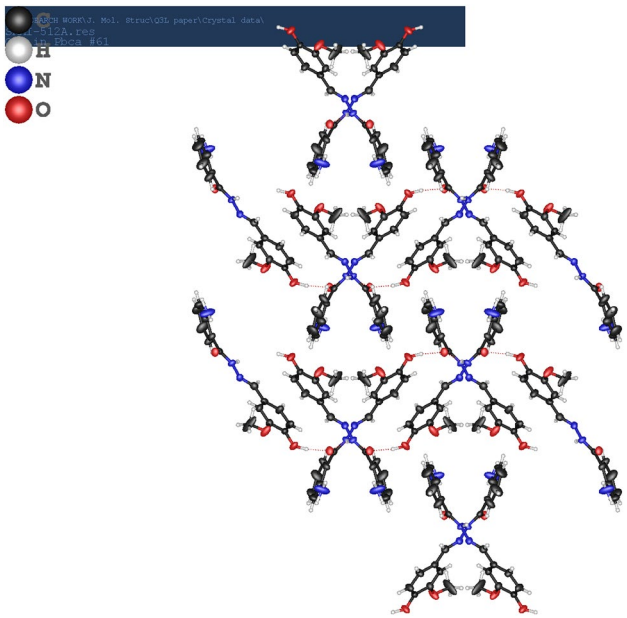

Figure 2. Crystal packing diagram of H-AHMB along b.

(NH) is also observed as a singlet at 6.4 ppm. The aromatic protons were clearly identified by observation at their respective places. The ^{13}C-NMR was also assigned without any constrains to the respective positions. The six quaternary carbon nuclei were observed viz; C=O was observed at 165.9 ppm, C–OH was seen at 150 ppm position and the Schiff base linkage was seen at 149.6 ppm. Rest of the spectrum is assigned to the respective carbon atoms.

Vibrational study

IR spectroscopic analysis was also performed to reveal the vibrations (figure 4S-8S). A sharp band at 3369 cm^{-1} was observed suggesting the involvement of $–NH_2$ moiety in the intramolecular hydrogen bonding as shown in Scheme 2.

Imine-iminium type of tautomerism is seen which lead to the vibration of NH only[46]. Hydroxyl group of vanillin is observed as a broad band at 3200 cm^{-1}. A vibrational mode for C=N is observed at 1641 cm^{-1} as a strong band. Whereas the NH_2 bends were observed as two bands at positions like 1616 cm^{-1} and 1604 cm^{-1}. The CH_3 bend is observed at 1440 cm^{-1} as medium band. The OH bend in plane was seen at 1350 cm^{-1} as a medium band and the out of the plane bend was observed at 730 cm^{-1} as a weak band.

All other bands were seen at their respective positions except for the moieties involved in coordination with metal centers. In case of Co-AHMB complex the NH_2 bands were observed at 3369 cm^{-1} and with shoulder peak whereas the band at 3216 cm^{-1} was displaced to 3180 cm^{-1} in Co-AHMB. Similarly, the ketone vibrational band was found missing in the Co-AHMB metal complex. The C=N band has been observed at 1641 cm^{-1} as was in ligand. Most likely the coordination in case of Co-AHMB complex may be assigned to the C=N and –OH groups as shown in Fig. 3.

Hence a kind of coordination polymer may be seen with distorted square planar /tetrahedral orientation. The structure may be concluded exactly upon successful crystallization from saturated solution. Till now all the attempts toward crystal growth were not fruitful.

Representative bands in case of Ni-AHMB complex were displaced to lower wavenumbers representing coordination. These include bands at 1641 cm^{-1} which have been affected to a greater extent and is converted to weak band. Similarly, the two pairs of bands have been displaced to 1614 cm^{-1} and 1598 cm^{-1} revealing $\Delta\lambda = 2$ to 6 cm^{-1}. The –OH band has also been effected and look absent or submerged in the region of 3200–3400 cm^{-1}. These two observations are pointing toward the coordination through NH_2 and C=N group. This conclusion is

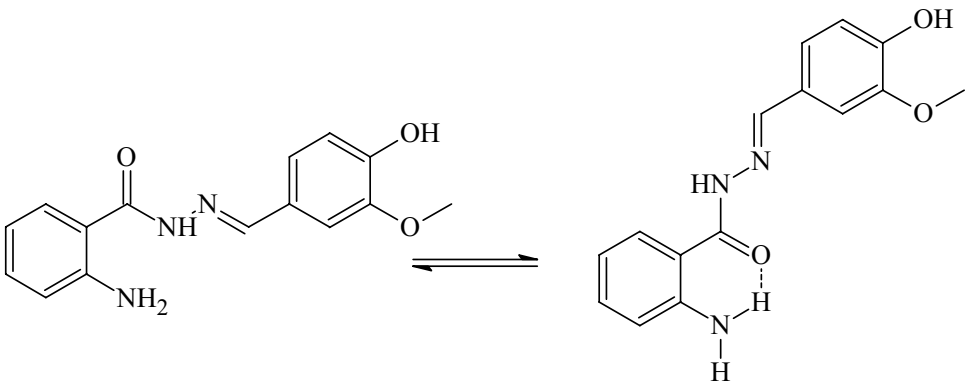

Scheme 2. Intermolecular hydrogen bonding in H-AHMB.

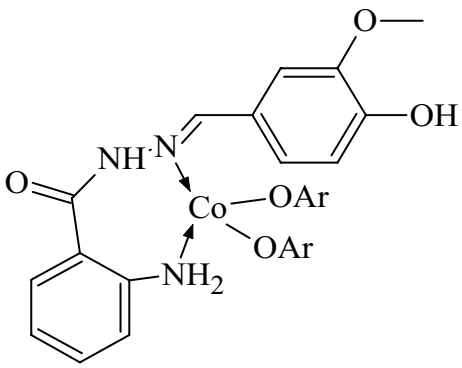

Figure 3. Co-AHMB complex.

further supported by disappearance of shoulder peak at 3200 cm^{-1}. Overall, coordination in case of Ni–AHMB complex is like the Co-AHMB complex.

Cu-AHMB complex with the hydrazide Schiff base ligand is not different than the cobalt and nickel derivatives. The differences seen here in Cu-AHMB complex were absence or broadening of –OH band, the absence of band responsible for C=N and the shift in the pair of bands {1610 cm^{-1} and 1600 cm^{-1}}. The bands responsible for in plane and out plane bends of –OH are completely absent. Zn-complex is exactly similar in coordination with Schiff base ligand as was Co-AHMB complex. Therefore, no need for further explanation. All the metal complexes were studied for elemental composition and close alignment of the calculated and found values show the formation of synthesized complexes.

Hirshfeld surface analysis

The intermolecular interactions in the crystal of H-AHMB can be affirmed from studying the Hirshfeld surface analysis. Intermolecular interactions are of immense importance in studying enzymatic interactions of the test compound and the active sites. Stronger intermolecular interactions in the crystal lattice is shown as red patches on the d_{norm} surface plot. The computation of the d_{norm} surface plot is done by measuring the d_e (external)and d_i (internal) distances to the nearby atoms.

The Hirshfeld surface area of H-AHMB ligand covers area of 346.70 $Å^2$ and spread over 357.41 $Å^3$ volume. The isovalue was found to be 0.5 with 0.701 globularity. The scaled colored patched index of H-AHMB can be seen in Fig. 4 whereas the quantitative and envisage of 2D fingerprint plot may be seen in Fig. 5. The short atomic contacts H···H = 39.9%, C···C = 2.6%, C···H = 15.8%, C···N = 0.5%, and H···O = 9.6% suggest that the major supports are from H···H, C···H and H···O compared to the other atomic interactions[65–70].

β-Glucuronidase inhibition

New metal based inhibitor particularly designed by combining essential metals with the organic substrates will definitely help to overcome the effects as mentioned in "Introduction" section caused by overly expressed β-glucuronides enzyme. Obviously such an inhibitor will reveal the value of metal ions as a novel strategy to overcome the overly expressed β-glucuronides enzyme. Herein, we are reporting the inhibition of β-glucuronidase enzyme by the metal complex derivatives of N′-[(4-hydroxy-3-methoxyphenyl)methylidene]-2-aminobenzohydrazide (H-AHMB). The results are tabulated in Table 3 and compared with D-saccharic acid-1,4-lactone. The Schiff base ligand H-AHMB and its metal derivatives were found active against the β-glucuronidase enzyme. Comparing the activity of the ligand with the metal derivatives it may be clarified that metal derivatives are more active than the neat ligand. From cobalt to zinc all the metal derivatives reveal similar activities. Interestingly, the inhibitory activity of all the metal derivatives are more than the standard drug used. It is apparent that upon complexation the activity is more enhanced. The nature of metal ion is also affecting the activity. For example zinc is enhancing the inhibition more than the other metal ions. Similarly, cobalt is following the zinc in inhibitory activity. By comparison, it is clear that Zn-AHMB is almost three times more effective than standard drug already in use. Whereas, Co-AHMB is active more than two folds against β-glucuronides enzyme in comparison to the standard drug. Other, metal complexes like Cu-AHMB is also very active with $IC_{50} = 32.3 \pm 1.00$ µM. And Ni-AHMB is the least active metal complex. Activity of Zn-AHMB may be linked to the structural features of β-glucuronidase enzyme. The β-glucuronidase enzyme bears two glutamic acid as active sites, zinc center is more Lewis acidic than the other metal ions and can actively react with O-containing sites hence, stopping the activity[71]. Similarly, cobalt is present in + 2 oxidation state which bears less Lewis acidity

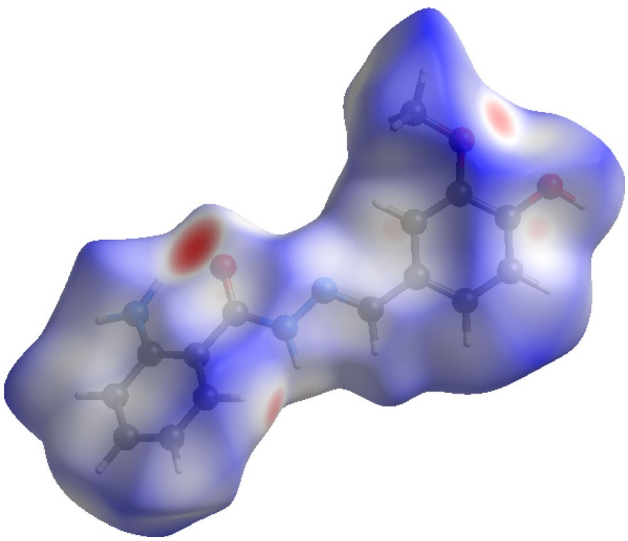

Figure 4. d_{norm} plot decorated Hirshfeld surface in different direction of lattice of H-AHMB.

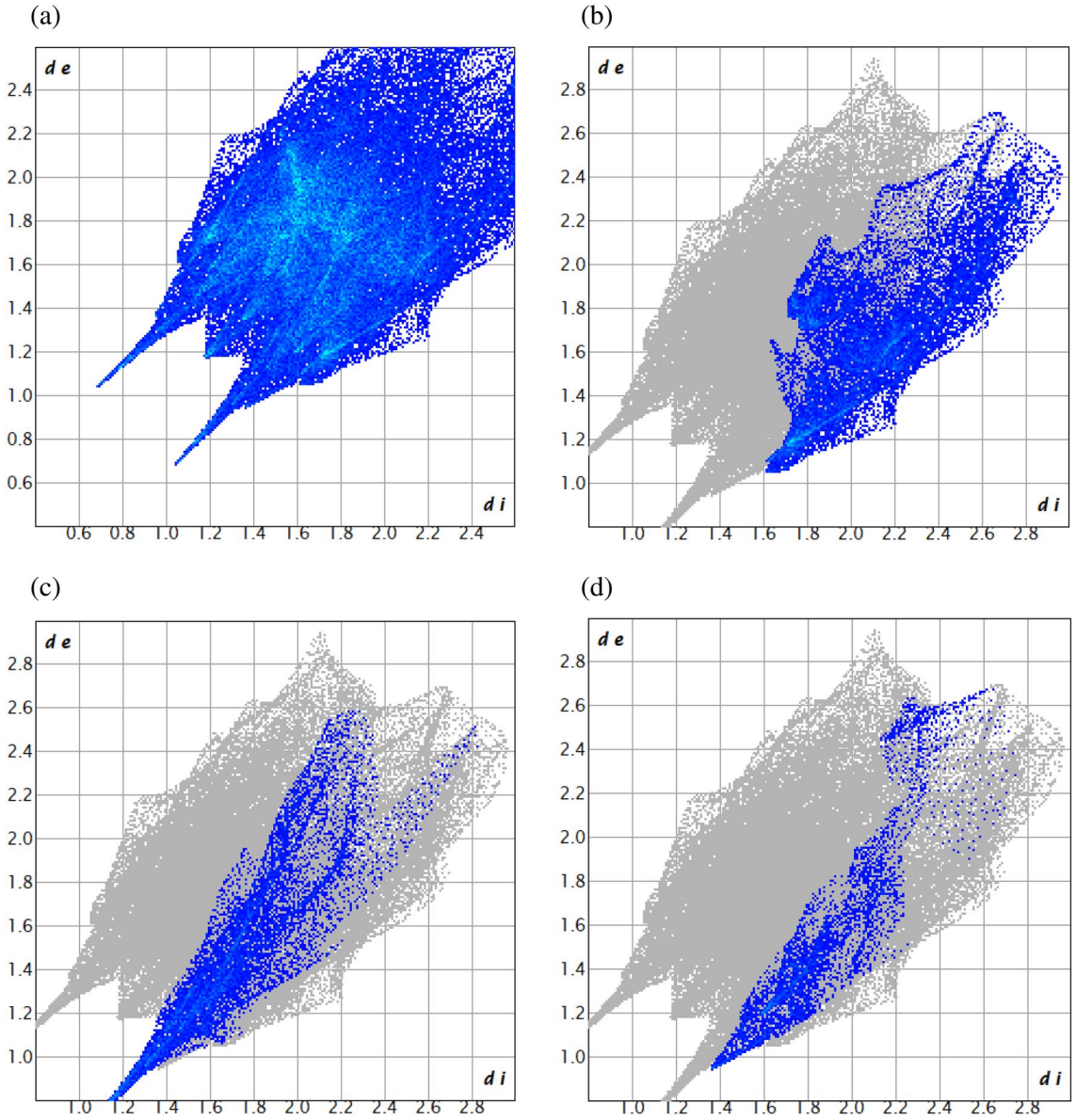

Figure 5. 2D fingerprint plots of short intermolecular interaction with their associate contributions to the HS in the crystal lattice of H-AHMB (**a**) all atoms interactions (**b**) C ···H/H ···C (**c**) O ···H/H ···O (d) N ···H/H ···N.

Compound	Conc. (mM)	% inhibition	$IC_{50} \pm SEM$ (µM)
H-AHMB	0.05	86.2	280.6 ± 2.02
Co-AHMB	0.05	78.8	21.7 ± 2.54
Ni-AHMB	0.05	96.0	40.59 ± 1.20
Cu-AHMB	0.05	73.3	32.3 ± 1.00
Zn-AHMB	0.05	98.3	17.3 ± 0.68
D-saccharic acid-1,4-lactone	0.05	89.4	45.75 ± 2.16

Table 3. β-Glucuronidase inhibition by H-AHMB and its metal derivatives.

than zinc center, therefore activity is less pronounced[71]. The less activity of nickel may be linked to its less binding potentials to carboxylic acid moieties in comparison to N-terminus amino acids and other nitrogenous substrates.

In conclusion, metal based β-glucuronidase inhibitor can be designed through the reaction of hydrazide based Schiff base ligand with essential metal ions.

Compound	Conc. (mM)	% Radical scavenging activity	$IC_{50} \pm SEM$ (μM)
H-AHMB	0.05	22.97	–
Co-AHMB	0.05	88.46	98.2 ± 1.78
Ni-AHMB	0.05	52.40	467 ± 2.90
Cu-AHMB	0.05	84.29	183 ± 6.60
Zn-AHMB	0.05	49.16	–
Gallic acid	0.05	93.13	63.0 ± 0.43

Table 4. DPPH scavenging activity by H-AHMB and its metal derivatives.

Free radical scavenging activities

Free radicals are short lived species bearing unpaired electrons and are usually produced inside mitochondria. Major free radicals are peroxide, superoxide ions, nitrates or peroxy nitrates. Many biological problems like ageing, rheumatoid arthritis, AIDS, cancer and neurodegenerative diseases are linked to free radicals or their effects[72]. Therefore, stopping their activities will be helpful in overcoming many diseases. Developing a successful antioxidant is an active area of research. Antioxidant substances bear hydrogen atoms or peroxide decomposers or oxygen quencher. Biological systems are supplied with natural antioxidants like glutathione, vitamin C, superoxide dismutases etc. Metal derivatives are supposed to be the better antioxidants which will definitely play role in increasing shelf life of industrial products.

Therefore, here we are also finding out the antioxidant potential of H-AHMB and its metal complexes against DPPH free radicals. Table 4 reveal the antioxidant potential of H-AHMB and its metal complexes. The ligand H-AHMB is inactive on its own whereas, except Zn-AHMB all the metal derivatives shown DPPH free radical scavenging activities. Among the active metal derivatives Co-AHMB with $IC_{50} = 98.2 \pm 1.78$ μM is the most active complex whereas, other metal derivatives were found weakly active. The activity of cobalt containing complex may be linked to its structural features where the C=N moiety seems to be free and may be involved in abstracting the proton of DPPH free radical[73]. The activity of Co-AHMB complex is less than the activity shown by gallic acid used as standard.

Conclusion

The ligand N′-[(4-hydroxy-3-methoxyphenyl)methylidene]-2-aminobenzohydrazide (H-AHMB) was synthesized from O-vanillin and 2-aminobenzohydrazide. It had been fully and well characterized prior to its complexation with metal ions like Co^{2+}, Ni^{2+}, Cu^{2+} and Zn^{2+}. The characterization techniques included FTIR, high resolution ESI(+) mass spectral analysis, ^{1}H and ^{13}C-NMR and single crystal diffraction analysis. All the spectral analysis confirm the formation of the ligand H-AHMB. The crystal data revealed orthorhombic, *Pbca* space group. Hirshfeld surface analysis revealed major interactions H…H, O…H and C…H confirming the hydrogen bonds in H-AHMB. The metal derivatives were prepared by reacting metal (II) chlorides with H-AHMB ligand. Elemental analyses, FTIR and UV/vis studies were carried out to confirm the metal and H-AHMB bonding. Single and diffractable crystals cannot be grown therefore, complete structural analysis will be reported in case of crystal growth. *β*-glucuronidase enzyme inhibition and DPPH free radical scavenging capabilities were also studied. Among the synthesized compounds Zn-AHMB with $IC_{50} = 17.3 \pm 0.68$ μM was found with greater efficiency than the standard drug in inhibiting the *β*-glucuronidase enzyme. Whereas, in DPPH radical scavenging capabilities Co-AHMB with $IC_{50} = 98.2 \pm 1.78$ μM was found most active in stopping DPPH free radicals. But the activity of Co-AHMB was found less than the standard drug. Overall, metallo *β*-glucuronidase inhibiting drug can be designed successfully using the H-AHMB ligand.

Data availability

NMR and IR spectral data is contained within the supplementary material. Crystallographic details are supplied in the supplementary information file and the structure was submitted to the CCDC. Data can be obtained free of charge from the Cambridge Crystallographic Data Centre by FAX (+44-1223-336-033), email (deposit@ccdc.cam.ac.uk) or their web interface (at http://www.ccdc.cam.ac.uk) by quoting the CCDC-number 2281686 for H-AHMB.

Received: 16 August 2023; Accepted: 13 December 2023
Published online: 04 January 2024

References

1. Asano, N. Glycosidase inhibitors: Update and perspectives on practical use. *Glycobiology* **13**, 93R – 104 (2003).
2. Gruner, S. A. W., Locardi, E., Lohof, E. & Kessler, H. Carbohydrate-based mimetics in drug design: Sugar amino acids and carbohydrate scaffolds. *Chem. Rev.* **102**, 491–514 (2002).
3. Leiria Campo, V., Aragão-Leoneti, V. & Carvalho, I. Glycosidases and diabetes: metabolic changes, mode of action and therapeutic perspectives. 181–203 (2013). https://doi.org/10.1039/9781849737173-00181.
4. Fishman, W. H. *Beta-Glucuronidase*. 361–409 (2006). https://doi.org/10.1002/9780470122617.ch7.
5. Whitaker, B. L. Plasma β-glucuronidase levels in breast cancer. *Br. J. Cancer* **14**, 471–477 (1960).
6. Odell, L. D. & Burt, J. C. Beta-glucuronidase activity in human female genital cancer. *Cancer Res.* **9**, 362–365 (1949).
7. Kim, D. H. & Jin, Y. H. Intestinal bacterial beta-glucuronidase activity of patients with colon cancer. *Arch. Pharm. Res.* **24**, 564–567 (2001).

8. Schumacher, U., Adam, E., Zangemeister-Wittkel, U. & Gossrau, R. Histochemistry of therapeutically relevant enzymes in human tumours transplanted into severe combined immunodeficient (SCID) mice: Nitric oxide synthase—associated diaphorase, β-D-glucuronidase and nonspecific alkaline phosphatase. *Acta Histochem.* **98**, 381–387 (1996).
9. Vlacha, V., Eliopoulou, M., Haidas, S. & Beratis, N. G. Correlation of cerebrospinal fluid β-glucuronidase activity with plasma methotrexate concentrations in leukemic children receiving high-dose methotrexate. *Pediatr. Blood Cancer* **42**, 350–356 (2004).
10. Gonick, H. C. Urinary ß-glucuronidase activity in renal disease. *Arch. Intern. Med.* **132**, 63 (1973).
11. Miller, B. F. Increase of serum β-glucuronidase activity in human diabetes mellitus. *JAMA* **195**, 189 (1966).
12. Rose, G. P., Dewar, A. J. & Stratford, I. J. A biochemical method for assessing the neurotoxic effects of misonidazole in the rat. *Br. J. Cancer* **42**, 890–899 (1980).
13. Saha, A. K., Glew, R. H., Kotler, D. P. & Omene, J. A. Elevated serum β-glucuronidase activity in acquired immunodeficiency syndrome. *Clin. Chim. Acta* **199**, 311–316 (1991).
14. Ganguly, N. K. *et al.* Acid hydrolases in monocytes from patients with inflammatory bowel disease, chronic liver disease, and rheumatoid arthritis. *Lancet* **1**, 1073–1075 (1978).
15. Westaway, M. S., Rheeder, P. & Guloba, G. Rheumatoid arthritis functional disability in a public health care clinic. *S. Afr. Med. J.* **98**, 706 (2008).
16. Boyland, E., Wallace, D. M. & Williams, D. C. Enzyme activity in relation to cancer. *Br. J. Cancer* **11**, 578–589 (1957).
17. Sloane, B. F., Dunn, J. R. & Honn, K. V. Lysosomal cathepsin B: Correlation with metastatic potential. *Science* **1979**(212), 1151–1153 (1981).
18. Southerland, J. H., Taylor, G. W. & Offenbacher, S. Diabetes and periodontal infection: Making the connection. *Clin. Diabetes* **23**, 171–178 (2005).
19. Llambés, F. Relationship between diabetes and periodontal infection. *World J. Diabetes* **6**, 927 (2015).
20. Henson, P. M. Pathologic mechanisms in neutrophil-mediated injury. *Am. J. Pathol.* **68**, 593–612 (1972).
21. Cui, G. *et al.* Synthesis and characterization of phenylboronic acid-containing polymer for glucose-triggered drug delivery+. *Sci. Technol. Adv. Mater.* **21**, 1–10 (2020).
22. Hsieh, H. K., Lee, T. H., Wang, J. P., Wang, J. J. & Lin, C. N. Synthesis and anti-inflammatory effect of chalcones and related compounds. *Pharm. Res.* **15**, 39–46 (1998).
23. Levvy, G. A. The preparation and properties of beta-glucuronidase. IV. Inhibition by sugar acids and their lactones. *Biochem. J.* **52**, 464–472 (1952).
24. Morita,. Effects of synthetic and natural in vivo inhibitors of β-glucuronidase on azoxymethane-induced colon carcinogenesis in rats. *Mol. Med. Rep.* https://doi.org/10.3892/mmr_00000022 (2008).
25. Pellock, S. J. *et al.* Gut microbial β-glucuronidase inhibition via catalytic cycle interception. *ACS Cent. Sci.* **4**, 868–879 (2018).
26. Kargar, H. *et al.* Synthesis, spectral characterization, SC-XRD, HSA, DFT and catalytic activity of novel dioxovanadium(V) complex with aminobenzohydrazone Schiff base ligand: An experimental and theoretical approach. *Inorganica Chim. Acta* **526**, 120535 (2021).
27. Kargar, H. *et al.* Titanium(IV) complex containing ONO-tridentate Schiff base ligand: Synthesis, crystal structure determination, Hirshfeld surface analysis, spectral characterization, theoretical and computational studies. *J. Mol. Struct.* **1241**, 130653 (2021).
28. Kargar, H. & Fallah-Mehrjardi, M. Novel dioxomolybdenum complexes containing ONO-tridentate Schiff base ligands derived from 4-aminobenzohydrazide: Synthesis, spectral characterization, and application as efficient homogeneous catalysts for selective sulfoxidation. *J. Iran. Chem. Soc.* **18**, 3443–3456 (2021).
29. Kargar, H. *et al.* Synthesis, crystal structure determination, Hirshfeld surface analysis, spectral characterization, theoretical and computational studies of titanium(IV) Schiff base complex. *J. Coord. Chem.* **74**, 2682–2700 (2021).
30. Kargar, H., Fallah-Mehrjardi, M., Behjatmanesh-Ardakani, R. & Munawar, K. S. Synthesis, spectra (FT-IR, NMR) investigations, DFT, FMO, MEP, NBO analysis and catalytic activity of MoO_2(VI) complex with ONO tridentate hydrazone Schiff base ligand. *J. Mol. Struct.* **1245**, 131259 (2021).
31. Kargar, H. *et al.* Synthesis, spectral characterization, SC-XRD, HSA, DFT and catalytic activity of a dioxidomolybdenum complex with aminosalicyl-hydrazone Schiff base ligand: An experimental and theoretical approach. *Polyhedron* **208**, 115428 (2021).
32. Malekshah, R. E., Shakeri, F., Aallaei, M., Hemati, M. & Khaleghian, A. Biological evaluation, proposed molecular mechanism through docking and molecular dynamic simulation of derivatives of chitosan. *Int. J. Biol. Macromol.* **166**, 948–966 (2021).
33. Parvarinezhad, S., Salehi, M., Kubicki, M. & Eshaghi Malekshah, R. Synthesis, characterization, spectral studies and evaluation of noncovalent interactions in co-crystal of μ-oxobridged polymeric copper(II) complex derived from pyrazolone by theoretical studies. *J. Mol. Struct.* **1260**, 132780 (2022).
34. Iraji, M., Salehi, M., Malekshah, R. E., Khaleghian, A. & Shamsi, F. Liposomal formulation of new arsenic schiff base complex as drug delivery agent in the treatment of acute promyelocytic leukemia and quantum chemical and docking calculations. *J. Drug Deliv. Sci. Technol.* **75**, 103600 (2022).
35. Cui, G. *et al.* Synthesis and characterization of Eu(III) complexes of modified D-glucosamine and poly(N-isopropylacrylamide). *Mater. Sci. Eng. C* **78**, 603–608 (2017).
36. Xu, H. *et al.* Atractylenolide I enhances responsiveness to immune checkpoint blockade therapy by activating tumor antigen presentation. *J. Clin. Investig.* https://doi.org/10.1172/JCI146832 (2021).
37. Yu, T. *et al.* Identification of potential biomarkers and pathways associated with carotid atherosclerotic plaques in type 2 diabetes mellitus: A transcriptomics study. *Front. Endocrinol.* https://doi.org/10.3389/fendo.2022.981100 (2022).
38. Wang, B., Xiang, J., He, B., Tan, S. & Zhou, W. Enhancing bioavailability of natural extracts for nutritional applications through dry powder inhalers (DPI) spray drying: technological advancements and future directions. *Front. Nutr.* https://doi.org/10.3389/fnut.2023.1190912 (2023).
39. Huang, S. *et al.* Targeting nano-regulator based on metal–organic frameworks for enhanced immunotherapy of bone metastatic prostate cancer. *Cancer Nanotechnol.* **14**, 43 (2023).
40. Wang, Y., Zhai, W., Cheng, S., Li, J. & Zhang, H. Surface-functionalized design of blood-contacting biomaterials for preventing coagulation and promoting hemostasis. *Friction* **11**, 1371–1394 (2023).
41. Xia, J. *et al.* Synthesis and biological activities of oxazolidinone pleuromutilin derivatives as a potent anti-MRSA agent. *ACS Infect. Dis.* **9**, 1711–1729 (2023).
42. Ji, Z. *et al.* Emergency treatment and photoacoustic assessment of spinal cord injury using reversible dual-signal transform-based selenium antioxidant. *Small* https://doi.org/10.1002/smll.202207888 (2023).
43. Zhao, Z. *et al.* Single-atom Fe nanozymes coupling with atomic clusters as superior oxidase mimics for ratiometric fluorescence detection. *Chem. Eng. J.* **469**, 143923 (2023).
44. Kong, L. *et al.* Enhanced red luminescence in $CaAl_{12}O_{19}$: Mn^{4+} *via* doping Ga^{3+} for plant growth lighting. *Dalton Trans.* **49**, 1947–1954 (2020).
45. Li, H. *et al.* Hexafluoroisopropanol based silk fibroin coatings on AZ31 biometals with enhanced adhesion, corrosion resistance and biocompatibility. *Prog. Org. Coat.* **184**, 107881 (2023).
46. Kong, L. & Liu, G. Synchrotron-based infrared microspectroscopy under high pressure: An introduction. *Matter Radiat. Extremes* https://doi.org/10.1063/5.0071856 (2021).
47. Cui, G. *et al.* Synthesis and characterization of Eu(III) complexes of modified cellulose and poly(N-isopropylacrylamide). *Carbohydr. Polym.* **94**, 77–81 (2013).

48. Wang, Y. *et al.* Friction behavior of biodegradable electrospun polyester nanofibrous membranes. *Tribol. Int.* **188**, 108891 (2023).
49. Lu, J. *et al.* A 4arm-PEG macromolecule crosslinked chitosan hydrogels as antibacterial wound dressing. *Carbohydr. Polym.* **277**, 118871 (2022).
50. Yang, Y., Shi, L., Li, J., Yao, L. & Xiang, D. Piperazine ferulate ameliorates the development of diabetic nephropathy by regulating endothelial nitric oxide synthase. *Mol. Med. Rep.* https://doi.org/10.3892/mmr.2019.9875 (2019).
51. Mi, W., Xia, Y. & Bian, Y. Meta-analysis of the association between aldose reductase gene (CA)n microsatellite variants and risk of diabetic retinopathy. *Exp. Ther. Med.* https://doi.org/10.3892/etm.2019.8086 (2019).
52. Huang, H. *et al.* The behavior between fluid and structure from coupling system of bile, bile duct, and polydioxanone biliary stent: A numerical method. *Med. Eng. Phys.* **113**, 103966 (2023).
53. Zhao, P. *et al.* Theoretical and experimental investigations on the phase stability and fabrication of high-entropy monoborides. *J. Eur. Ceram. Soc.* **43**, 2320–2330 (2023).
54. Wang, L. *et al.* Regulating the alkyl chain length of quaternary ammonium salt to enhance the inkjet printing performance on cationic cotton fabric with reactive dye ink. *ACS Appl. Mater. Interfaces* **15**, 19750–19760 (2023).
55. Zhang, Y., Zhao, M., Huang, J., Zhao, N. & Yu, H. Controllable synthesis, photocatalytic property, and mechanism of a novel POM-based direct Z-scheme nano-heterojunction α-Fe_2O_3/P_2Mo_{18}. *Molecules* **28**, 6671 (2023).
56. Xiao, Y., Gong, W., Zhao, M., Zhang, M. & Lu, N. Surface-engineered prussian blue nanozymes as artificial receptors for universal pattern recognition of metal ions and proteins. *Sens. Actuators B Chem.* **390**, 134006 (2023).
57. Parvarinezhad, S., Salehi, M., Kubicki, M. & Eshaghi Malekshah, R. Experimental and theoretical studies of new Co(III) complexes of hydrazide derivatives proposed as multi-target inhibitors of SARS-CoV-2. *Appl. Organomet. Chem.* https://doi.org/10.1002/aoc.6836 (2022).
58. Ikram, M. *et al.* Synthesis, spectral, Hirshfeld surface analysis and biological evaluation of a Schiff base copper(II) complex: Towards a copper(II) based human anti-glioblastoma agent. *J. Mol. Struct.* **1278**, 134960 (2023).
59. Ikram, M., Rehman, S., Akhtar, M. N., Subhan, F. & Aslam, S. Selective urease inhibitory and antimicrobial activities of transition metal complexes of amino acid bearing Schiff base ligand: Thermal degradation behavior of complexes. *Pharm. Chem. J.* **54**, 469–477 (2020).
60. Ikram, M. *et al.* Synthesis, characterization, antioxidant and selective xanthine oxidase inhibitory studies of transition metal complexes of novel amino acid bearing Schiff base ligand. *Inorganica Chim. Acta* **428**, 117–126 (2015).
61. Ikram, M., Rehman, S., Subhan, F., Akhtar, M. N. & Sinnokrot, M. O. Synthesis, characterization, thermal degradation and urease inhibitory studies of the new hydrazide based Schiff base ligand 2-(2-hydroxyphenyl)-3-{[(E)-(2-hydroxyphenyl)methylidene] amino}-2,3-dihydroquinazolin-4(1H)-one. *Open Chem.* **15**, 308–319 (2017).
62. Dolomanov, O. V., Bourhis, L. J., Gildea, R. J., Howard, J. A. K. & Puschmann, H. OLEX2: A complete structure solution, refinement and analysis program. *J. Appl. Crystallogr.* **42**, 339–341 (2009).
63. Bourhis, L. J., Dolomanov, O. V., Gildea, R. J., Howard, J. A. K. & Puschmann, H. The anatomy of a comprehensive constrained, restrained refinement program for the modern computing environment—Olex2 dissected. *Acta Crystallogr. A Found Adv.* **71**, 59–75 (2015).
64. Soare, J. R., Dinis, T. C. P., Cunha, A. P. & Almeida, L. Antioxidant activities of some extracts of *Thymus zygis*. *Free Radic. Res.* **26**, 469–478 (1997).
65. Simsek, O., Ashfaq, M., Tahir, M. N., Ozturk, S. & Agar, E. Synthesis and charaterizations of the Schiff base derived from 2-hydroxy-5-nitrobenzaldehyde alongwith Hirshfeld surface analysis and computational study. *J. Struct. Chem.* **64**, 942–953 (2023).
66. Kansız, S. & Dege, N. Synthesis, crystallographic structure, DFT calculations and Hirshfeld surface analysis of a fumarate bridged Co(II) coordination polymer. *J. Mol. Struct.* **1173**, 42–51 (2018).
67. Kargar, H. *et al.* Sonication-assisted synthesis of new Schiff bases derived from 3-ethoxysalicylaldehyde: Crystal structure determination, Hirshfeld surface analysis, theoretical calculations and spectroscopic studies. *J. Mol. Struct.* **1243**, 130782 (2021).
68. Ashfaq, M., Nawaz Tahir, M., Munawar, K. S., Behjatmanesh-Ardakani, R. & Kargar, H. Single crystal exploration, supramolecular behaviour, Hirshfeld surface analysis, linear and non-linear theoretical optical properties of Schiff bases derived from Benzene sulfonamides. *J. Mol. Struct.* **1261**, 132952 (2022).
69. Kargar, H. *et al.* Theoretical studies, Hirshfeld surface analysis, and crystal structure determination of a newly synthesized benzothiazole copper(II) complex. *J. Mol. Struct.* **1261**, 132905 (2022).
70. Kargar, H. *et al.* Unsymmetrical Ni(II) Schiff base complex: Synthesis, spectral characterization, crystal structure analysis, Hirshfeld surface investigation, theoretical studies, and antibacterial activity. *J. Mol. Struct.* **1265**, 133381 (2022).
71. Kildahl, N. K. & Viriyanon, P. Lewis acidity of cobalt(I). *Inorg. Chem.* **26**, 4188–4194 (1987).
72. Awolade, P. *et al.* Therapeutic significance of β-glucuronidase activity and its inhibitors: A review. *Eur. J. Med. Chem.* **187**, 111921 (2020).
73. Demir, S. *et al.* A novel 3-acetoxy-2-methyl-N-(4-methoxyphenyl)benzamide: Molecular structural describe, antioxidant activity with use X-ray diffractions and DFT calculations. *J. Mol. Struct.* **1100**, 582–591 (2015).

Acknowledgements

This research was supported by grants from the Higher Education Commission Pakistan {NRPU sponsored project no. Ref No. 20-14898/NRPU/R&D/HEC/2021-2020} and Abdul Wali Khan University Mardan Pakistan. Authors are thankful to the researchers supporting project number [RSP2024R235], King Saud University, Riyadh, Saudi Arabia.

Author contributions

A.K. conceived and designed the experiments; M.I., Farzia, R.K., F.A., M.A., A.F.A.; performed the experiments; M.I., S.R., Farzia, and A.K.; analyzed and interpreted the data; M.I., S.R., Farzia, M.K., M.O.S., A.F.A., F.A., M.A.; contributed reagents, materials, analysis tools or data; M.I., S.R., A.K., M.O.S. and R.K.; wrote the paper. All authors reviewed the manuscript.

Competing interests

The authors declare no competing interests.

Additional information

Supplementary Information The online version contains supplementary material available at https://doi.org/10.1038/s41598-023-49893-6.

Correspondence and requests for materials should be addressed to S.R., M.I. or A.K.